Soft Matter

COMMUNICATION

View Article Online
View Journal | View Issue

Cite this: *Soft Matter*, 2019, **15**, 4609

Received 28th March 2019,
Accepted 18th May 2019

DOI: 10.1039/c9sm00630c

rsc.li/soft-matter-journal

Deformation of soft particles with controlled elasticity by liquid–liquid interfacial tension†

Benedikt Sapotta,[ab] Jongmin Q. Kim,[a] Norbert Willenbacher[b] and Siyoung Q. Choi *[a]

Herein we report the deformation of PDMS-based particles at a liquid–liquid interface at varying degrees of softness. Direct visualization of the particle adsorption to the interface reveals at least five different modes of deformation from the complete spreading of a polymer resin droplet to a non-deforming, rigid particle.

Pickering emulsions exploit the adsorption of particles to energy intensive liquid–liquid interfaces as a means to achieve interfacial stabilization. The stabilization effect increases with the amount of interfacial area covered by each individual particle. Therefore, the stabilization effect is maximized if a spherical particle is equally submerged into both liquid phases, which is commonly referred to as the neutral wetting state and depends on the wetting characteristics of the particle surface.[1–5]

An alternative approach to further boost interfacial coverage is the use of deformable particles which are stretched once in contact with a liquid–liquid interface.[6,7] Recently, Style *et al.* established a theoretical basis to understand the mechanical properties that govern particle deformation at liquid–liquid interfaces.[8] They demonstrated that the relationship between the initial particle radius, r_0, and the elastocapillary length, L_{el}, the ratio of interfacial tension to the particle's Young's modulus, is of pivotal importance. The larger the radius of a particle compared to its elastocapillary length the smaller the degree of deformation and thus the relative increase in interfacial coverage. Furthermore, under the assumption of linear elastic behaviour as well as partial wetting conditions, in which the sum of both particle–liquid interfacial tensions is larger than the interfacial tension of the liquid–liquid interface, they were able to compute the transition from a rigid particle ($r_0 \gg L_{el}$) that is not visibly deformed to a perfectly soft, liquid-like particle ($r_0 < L_{el}$) that forms a lenticular shape.[8] Going one step further, Mehrabian *et al.* applied the concept of elastocapillary length to the complete wetting case, in which the sum of interfacial tensions between a particle and both liquid phases is smaller than the interfacial tension of the liquid–liquid interface.[9] They argued that the deformed shape under complete wetting conditions cannot be described by continuum theory as molecular details become increasingly important. However, to date, there has been no concise theoretical framework to describe soft particle deformation under complete wetting conditions.

Experimentally, soft particle deformation at liquid–liquid interfaces under complete wetting conditions is already utilized most prominently in the form of poly(*N*-isopropylacrylamide) (PNIPAM) microgel particles as Pickering emulsion stabilizers.[6] PNIPAM microgels are functionalized hydrogel particles usually submicrometer in size, which swell in an aqueous phase, rendering them extremely soft. Destribats *et al.* showed that an increase in the crosslinking density of a PNIPAM microgel particle has a negative effect on emulsion stability,[10] thus demonstrating the significance of particle deformability when it comes to interfacial stabilization. Due to their uneven crosslinking density distribution, microgels are reported to deform to a polymer corona surrounding a mostly undeformed core. Geisel *et al.* used the freeze-fracture shadow-casting cryo-scanning-electron-microscopy to shed light on the 3D shape of the deformed microgel particles.[11] They found that with the exception of the core slightly protruding, the deformed microgel is largely flattened on the oil side. In contrast, the microgel is able to retain most of its original shape on the water side, meaning that the microgel particle is deformed in a radial direction upon contact with the interface without penetrating into the oil phase. However, due to their small size, visualizing deformed microgels at interfaces remains difficult.[12,13] Only the recent development of microgels up to a size of 6 μm allowed gaining further insight into the actual deformation kinetics based on fluorescence microscopy.[14] In general, the deformation of PNIPAM microgels at interfaces results from the interplay between interfacial tension, the swelling state, elasticity and deformability, all of which are inherently difficult to quantify.[7] Therefore, microgels are only of limited use as model

[a] *Department of Chemical and Biomolecular Engineering, Korea Advanced Institute of Science and Technology (KAIST), Daejeon, South Korea. E-mail: sqchoi@kaist.ac.kr*

[b] *Faculty of Chemical and Process Engineering, Karlsruhe Institute of Technology (KIT), Karlsruhe, Germany*

† Electronic supplementary information (ESI) available. See DOI: 10.1039/c9sm00630c

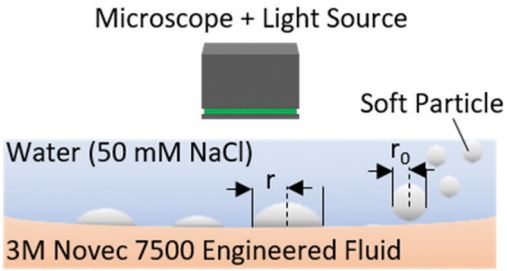

Fig. 1 Deformation bath containing the water–3M Novec 7500 Engineered Fluid interface. The PDMS-based particles were added to the water phase and sedimented to the interface. The particle radius before deformation, r_0, and the apparent equilibrium radius after deformation, r, were determined by image processing of the respective micrographs.

substances to further increase our theoretical understanding of soft particle deformation. The aim of this paper is to illustrate the connection between particle softness and deformation at a liquid–liquid interface under complete wetting conditions. For simplicity, we focus solely on the deformation of isolated particles (3.5 μm < r_0 < 35 μm) at a planar oil–water interface (o–w interface). The deformation event is captured by plain light microscopy as shown in Fig. 1. Further, the particles are hardened in the deformed state, then removed from the interface and later investigated using scanning electron microscopy (SEM). Measuring the complex shear modulus $G^* = G' + i{\cdot}G''$ of the particle's bulk material allows us to quantify its linear viscoelastic properties.

We used the commercially available two-component elastomer kit Sylgard 184 (which consists of a base and a curing agent that lead to a polydimethylsiloxane (PDMS) elastomer once mixed) as a model substance. The change in its mechanical properties during the curing reaction was tracked using an MCR 302 rheometer (Anton Paar, Austria). Measurements were carried out in the linear regime with a PP25 measuring plate, a strain rate of 1%, an angular frequency of 2π rad s^{-1} and a gap width of 200 μm. The sample was prepared by mixing the base and curing agent at the recommended weight ratio of 10 : 1 followed by a brief centrifugation to remove air bubbles.

The storage modulus, G', and loss modulus, G'', as functions of the curing time, t_{cure}, at the temperature T = 40 °C are displayed in Fig. 2A. The initially liquid PDMS resin mixture exhibits no elasticity. After $t_{cure} \sim 90$ min the influence of the curing reaction on the bulk elasticity reaches beyond the detection limit with the crossover of G'' and G' occurring after $t_{cure} = 153 \pm 3$ min. It must be noted that the exact location of the crossover point in Fig. 2A might indeed depend on the applied frequency and therefore not necessarily coincide with the actual gel point, *i.e.* the transition from a liquid to a solid.[15,16] To investigate the true rheological behaviour of our model material, we conducted a frequency sweep after t_{cure} = 180 min, which is displayed in Fig. 2B. During our deformation experiments, which will be explained further below, the timescale of deformation, until an equilibrium size was reached, ranged between 1 and 30 s. The frequency sweep in Fig. 2B and the creep compliance data shown in Fig. S4 (ESI†) clearly prove the solid-like behaviour of Sylgard 184 on the timescale of deformation, validating the applicability of the elastocapillary concept to our study.

To prepare soft Sylgard 184 particles dispersed in water, a base and a curing agent were mixed and subsequently emulsified in DI water with a Polytron PT 1300 D homogenizer (Kinematica, Switzerland) at 8000 rpm for 3 minutes. The water : base : curing agent weight ratio was 100 : 10 : 1. Immediately after preparation, the PDMS resin in the water emulsion was placed into a heated bath at T = 40 °C. Thermal quenching of emulsion samples taken at designated time intervals allowed us to prepare PDMS-based particles of varying mechanical strengths. Afterwards, the emulsion samples were added into a "deformation bath" featuring an interface between water and the Hydrofluoroether 3M Novec 7500 Engineered Fluid as displayed in Fig. 1. The 3M Novec 7500 Engineered Fluid was chosen to represent the oil phase due to its inertness and its density (ρ = 1.62 g cm^{-3} at 25 °C)[17]

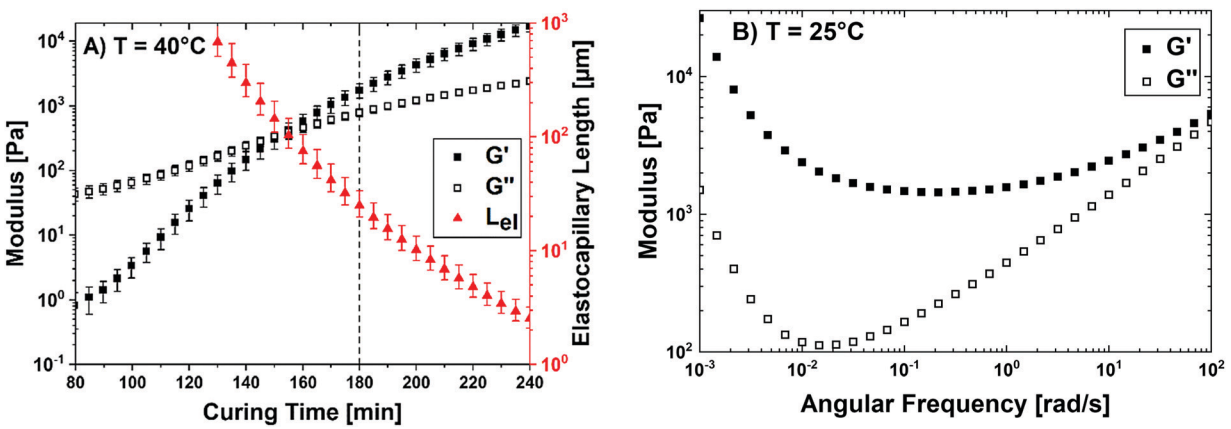

Fig. 2 (A) Storage modulus G' and loss modulus G'' of Sylgard 184 as functions of time at a curing temperature of 40 °C. In our study, we calculate the elastocapillary length, L_{el}, as the ratio of the o–w interfacial tension in the deformation bath to G'. The dashed line was added to highlight the curing state in which the frequency sweep shown in (B) was conducted. (B) Frequency sweep of Sylgard 184, which was cured for 180 min at 40 °C. The sample behaves solid-like ($G' > G''$) in the investigated frequency range. The increase in G' at small frequencies is caused by the continuing curing reaction since smaller ω values require longer measuring times (see Fig. S3, ESI†).

being larger than the density of water. The swelling of PDMS by both the oil and water phases is assumed to be negligible. Both the Sylgard 184 curing agent[18] and base[19] offer densities larger than 1 g cm^{-3}, which is why our PDMS-based particles sedimented to the o–w interface when added into the deformation bath. A background electrolyte of 50 mM NaCl was used in the water phase to facilitate the film drainage step between the sedimented particles and the interface, thus allowing particles to reach the interface more quickly. The light microscope was positioned above the deformation bath and image processing provided the respective particle radii. The apparent equilibrium radius after deformation was determined once the size of the deformed particles remained constant for at least 5 s.

To analyse our findings, we define the elastocapillary length, L_{el}, in our study as the ratio between the interfacial tension of the o–w interface, γ_{o-w}, and the storage modulus of the PDMS particles, $L_{el} = \gamma_{o-w}/G'$. The pendant drop method was used to experimentally determine γ_{o-w}, yielding a value of 43.5 $\pm$ 0.5 mN m^{-1}. The resulting elastocapillary length is plotted alongside the storage modulus in Fig. 2A. Further, we define the degree of deformation, D, as the ratio of the apparent particle radii after and before deformation $D = r/r_0$, as well as the elastocapillary ratio, R_{el}, as the ratio of the initial particle radius to the elastocapillary length $R_{el} = r_0/L_{el}$.

We categorize the particle response upon contact with the o–w interface into five different regimes. The first regime corresponds to the PDMS chains being not or insufficiently connected with each other. In this trivial case, the polymer particles behave liquid-like and completely spread on the o–w interface. Due to the lack of contrast, the size of the deformed shape in the first regime could not be determined with our light microscopy method. In general, the thickness of an isolated liquid layer at an interface formed under complete wetting conditions is larger than the molecular size.[20] On the other hand, PDMS chains are known to form monomolecular layers at the air–water-interface, which is commonly attributed to the amphiphilic nature of the siloxane groups,[21] and might also lead to a monomolecular layer at an o–w interface.

To our surprise, the particles appear to keep deforming to a thin film even after a curing time of 180 min, where elasticity dominates over viscosity, thus imparting yield stress to the particles. Assuming that the volume remains constant during deformation and that the deformed particles take a cylindrical shape, it is possible to estimate the deformed particle thickness, h, with $h = 4r_0/3D^2$. As shown in Fig. 3, concentric rings become visible on the deformed particle once the peak wavelength of our microscopy illumination system of 450 nm and h are in the same order of magnitude. Light reflected by the particle–water interface and light reflected by the particle–oil interface interfere with each other, causing constructive and destructive phase interaction, *i.e.* bright and dark fringes. The interference pattern observable during the second regime closely resembles Newton's rings, which are caused by light reflections at curved and flat interfaces. While we do not know the exact shape, we think a detailed study of this interesting phenomenon with a more monochromatic light source is likely to provide further insight

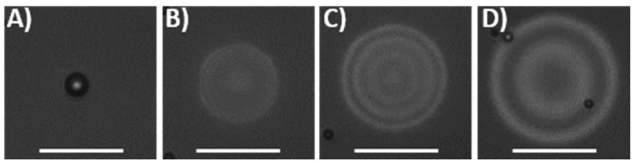

Fig. 3 Particle deformation in the second regime (r_0 = 7.1 μm) after t_{cure} = 180 min with dark and bright fringes visible on the deformed particle. The thickness h is calculated assuming a constant volume and a cylindrical shape of the deformed particle. (A) t = 0 s; (B) t = 0.63 s; r = 23.9 μm; h = 0.84 μm; (C) t = 1.96 s; r = 32.3 μm; h = 0.46 μm; and (D) t = 11 s; r = 39.5 μm; h = 0.31 μm (equilibrium size). The peak wavelength of the microscopy light is 450 nm (see Fig. S6 for more details, ESI†). The undeformed particles visible in (C) and (D) have not yet come into contact with the interface. The scale bar is 50 μm.

into the shape of the deformed particles,[22] which however would go beyond the scope of this work. Judging from the homogenous array of concentric rings, we presume that the particle is stretched relatively homogeneously in a radial direction once in contact with the o–w interface. In contrast to the first regime, the deformation in the second regime could be measured and is highlighted in Fig. 4. The second regime deformation could only be observed if the initial particle radius was clearly smaller than the corresponding elastocapillary length. However, there is only a minor correlation between deformation and the elastocapillary ratio, which might be caused by the relatively large influence of image processing uncertainties at large degrees of deformation. Also, considering the increase in particle radius of up to seven-fold, it is possible that the second regime deformation reaches beyond the elastic limit of the polymeric particles (see Fig. S4 for more information, ESI†).

The transition from the second to the third regime is marked with a dramatic decrease in deformation. Although our data are subject to modest scattering, the overall degree of deformation decreases with an increase in the elastocapillary

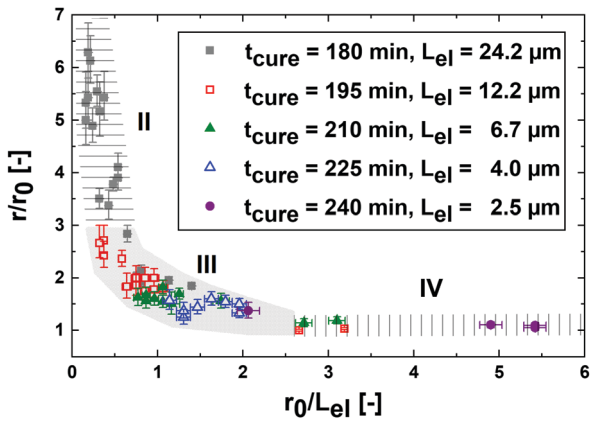

Fig. 4 Degree of deformation in relation to the elastocapillary ratio. There is only a minor correlation between the elastocapillary ratio and the observed degree of deformation in the second regime. While the degree of deformation decreases with an increase in the elastocapillary ratio in the third regime, almost no increase in the apparent particle radius can be detected in the fourth regime. The error bars account for the inaccuracy in image processing. The ESI† contains a detailed error analysis.

ratio across all sampling times in the third regime. Especially noteworthy is that the third regime covers the elastocapillary ratios from $\sim$0.5 to 2, where the particle radius and elastocapillary length are considerably close to each other. The distinguishing characteristic of the fourth regime is the overall lack of deformation when observed in our deformation bath. In fact, the contact event of the particle with the o–w interface features only a minor change in contrast, while the apparent particle size as observed under the light microscope remains almost unchanged.

By heating the deformed droplets at the interface, the curing reaction can be reinitiated, solidifying the deformed shape for further inspection using SEM. Preservation and deposition of the deformed particles on a solid substrate was successful for particles deformed in the third and fourth regimes. In contrast, SEM visualization of the strongly deformed particles in the second regime was not possible due to the interconnection of the individual particles, which can also be seen in Fig. 5. This interconnection is in fact consistent with the overall theory of soft particle deformation induced by interfacial forces. Provided that the o–w interfacial tension is in the same order of magnitude as the particle–liquid interfacial tension, the same mechanical properties that cause an adsorbed particle to be elastically deformed at the o–w interface also allow two particles to partially merge by undergoing arrested coalescence.[23] In other words, arrested coalescence could also be described as soft particle deformation at the particle–liquid interface. Although the particle interconnection complicates image analysis, the micrographs in Fig. 5 allow gaining further insight into the wetting behaviour of the PDMS-based particles as well as the conceptual differences in the third and fourth regimes.

As the sedimentation velocity increases with particle size, larger particles arrive at the o–w interface first, blocking further contact of smaller particles with the interface. Therefore, we can identify the blank faces without undeformed particles attached to it in Fig. 5 as the portion of the particle that is in contact with the oil phase.

Fully cured Sylgard 184 is considered highly hydrophobic.[24,25] However, with the curing process taking place while dispersed in the aqueous phase, our particles appear to adopt a more hydrophilic surface texture possibly caused by amphiphilic molecules being arrested in their hydrophilic surface orientation during the curing reaction. This may explain why the cured Sylgard 184 particles shown in Fig. 5 did not neutrally adsorb to the o–w interface but preferred interfacial contact with the water phase over the oil phase. Still, particle adsorption to the interface indicates that the o–w interfacial energy outweighs the oil–particle interfacial energy. However, from a geometrical point of view, the amount of o–w interfacial area covered by the adsorbed particle can only be equal to or smaller than the interfacial area between the adsorbed particle and the oil phase.

Fig. 5A displays the deformed state of particles in the third regime. The particle interfaces in contact with the oil phase are significantly larger than the cross section of the undeformed, spherical particle. In the deformed state, the particle takes the shape of a spherical cap with the interface in contact with the oil phase, exhibiting only a negligible amount of curvature, as was reported in microgel deformation.[10,11] In fact, the flattened interface offers maximum coverage of the o–w interface while minimizing the oil–particle interfacial area. However, as the particle stiffness increases, the interfacial energy gain attainable by particle deformation diminishes. This becomes evident in Fig. 5B representing the fourth regime where the particles do not maximize the o–w interfacial coverage as this would create a substantial amount of particle–oil interfacial area. The interfacial area protruding into the oil phase can no longer be flattened and its curvature increases with particle stiffness, ultimately converging to the fifth regime of a non-deforming, rigid particle.

Interestingly, we found no evidence pointing towards a fried-egg like structure as was reported for microgel deformation.[10] Presumably, the crosslinking density distribution of Sylgard 184 is more homogenous than in the case of microgels, which exhibit a soft shell and a more rigid core.[10]

In summary, we experimentally identified five different stages in particle deformation at a liquid–liquid interface under complete wetting conditions at varying degrees of softness for the first time. The silicone elastomer kit Sylgard 184 as a model material allowed full control over the mechanical properties of soft particles as well as visualization of particle deformation by

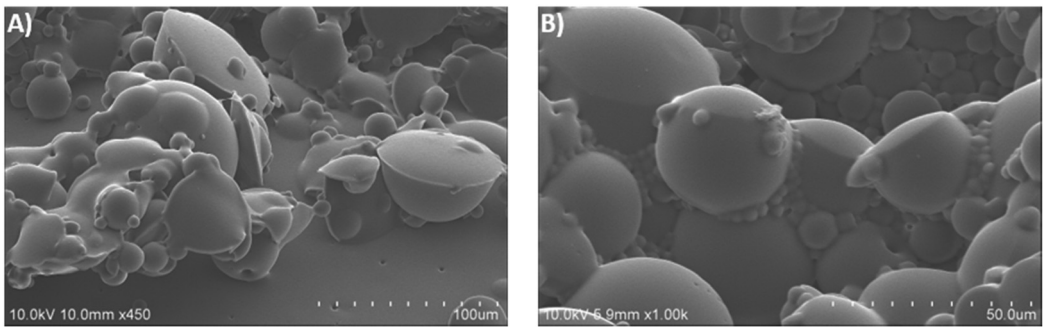

Fig. 5 SEM micrographs for particles deformed after (A) t_{cure} = 195 min (third regime) and (B) t_{cure} = 240 min (fourth regime). The blank faces with no undeformed particles attached were in contact with the oil phase. (A) Shows deformed particles in the third regime; the faces in contact with the oil phase are largely flattened. (B) Shows deformed particles in the fourth regime in which the apparent particle radius as observed in our deformation bath does not change upon deformation. The particles are connected to each other due to arrested coalescence.

mere light microscopy and, beyond that, preservation of the deformed shape through reinitiation of the curing reaction. Therefore, the particle reaction upon contact with the liquid–liquid interface could be classified as spreading in the case of a liquid-like particle; deformation to either a thin film ($r_0 < L_{el}$), a spherical cap ($r_0 \sim L_{el}$) or an assembly of two spherical caps ($r_0 > L_{el}$) or no visible deformation in the case of a rigid particle ($r_0 \gg L_{el}$). We are convinced that our findings will prove to be an important guideline for future research on soft particle deformation and eventually contribute to further enhance interfacial stabilization by soft particle adsorption.

Conflicts of interest

There are no conflicts to declare.

Acknowledgements

This work was supported by the Basic Science Research Program through the National Research Foundation of Korea (NRF-2015R1C1A1A01054180) as well as the Leading Foreign Research Institute Recruitment Program through the National Research Foundation of Korea funded by the Ministry of Science and ICT (MSIT) (NRF-2015K1A4A3047100). Benedikt Sapotta acknowledges the financial support granted by the German Federal Ministry of Education and Research (BMBF) through the German Academic Exchange Service (DAAD).

References

1 N. Ballard, A. D. Law and S. A. F. Bon, *Soft Matter*, 2019, **15**, 1186–1199.
2 Y. Chevalier and M.-A. Bolzinger, *Colloids Surf., A*, 2013, **439**, 23–34.
3 K. Kim, S. Kim, J. Ryu, J. Jeon, S. G. Jang, H. Kim, D. G. Gweon, W. B. Im, Y. Han, H. Kim and S. Q. Choi, *Nat. Commun.*, 2017, **8**, 14305.
4 S. Kim, K. Kim and S. Q. Choi, *Soft Matter*, 2018, **14**, 1094–1099.
5 S. Levine, B. Bowen and S. Partridge, *Colloids Surf.*, 1989, **38**, 325–343.
6 T. Ngai, S. H. Behrens and H. Auweter, *Chem. Commun.*, 2005, 331–333, DOI: 10.1039/b412330a.
7 W. Richtering, *Langmuir*, 2012, **28**, 17218–17229.
8 R. W. Style, L. Isa and E. R. Dufresne, *Soft Matter*, 2015, **11**, 7412–7419.
9 H. Mehrabian, J. Harting and J. H. Snoeijer, *Soft Matter*, 2016, **12**, 1062–1073.
10 M. Destribats, V. Lapeyre, M. Wolfs, E. Sellier, F. Leal-Calderon, V. Ravaine and V. Schmitt, *Soft Matter*, 2011, **7**, 7689–7698.
11 K. Geisel, L. Isa and W. Richtering, *Langmuir*, 2012, **28**, 15770–15776.
12 K. Geisel, K. Henzler, P. Guttmann and W. Richtering, *Langmuir*, 2015, **31**, 83–89.
13 S. Schmidt, T. Liu, S. Rutten, K. H. Phan, M. Moller and W. Richtering, *Langmuir*, 2011, **27**, 9801–9806.
14 H. Minato, M. Murai, T. Watanabe, S. Matsui, M. Takizawa, T. Kureha and D. Suzuki, *Chem. Commun.*, 2018, **54**, 932–935.
15 H. H. Winter and F. Chambon, *J. Rheol.*, 1986, **30**, 367–382.
16 H. H. Winter, *Polym. Eng. Sci.*, 1987, **27**, 1689–1702.
17 M. H. Rausch, L. Kretschmer, S. Will, A. Leipertz and A. P. Fröba, *J. Chem. Eng. Data*, 2015, **60**, 3759–3765.
18 *Sylgard 184 Silicone Elastomer Curing Agent – Safety Data Sheet. Issue Date 03/13/2018. The Dow Chemical Company*.
19 *Sylgard 184 Silicone Elastomer Base – Safety Data Sheet. Issue Date 03/27/2018. The Dow Chemical Company*.
20 P. G. de Gennes, *Rev. Mod. Phys.*, 1985, **57**, 827–863.
21 L. T. Lee, E. K. Mann, D. Langevin and B. Farnoux, *Langmuir*, 1991, **7**, 3076–3080.
22 C. Illueca, C. Vazquez, C. Hernández and V. Viqueira, *Ophthalmic Physiol Optic*, 1998, **18**, 360–371.
23 A. B. Pawar, M. Caggioni, R. W. Hartel and P. T. Spicer, *Faraday Discuss.*, 2012, **158**, 341–350.
24 K. Efimenko, W. E. Wallace and J. Genzer, *J. Colloid Interface Sci.*, 2002, **254**, 306–315.
25 F. Sabri, J. G. Marchetta, M. Sinden-Redding, J. J. Habenicht, T. C. Phung, C. N. Melton, C. J. Hatch and R. L. Lirette, *PLoS One*, 2012, **7**, e45719.